

1

APPROVED FOR PUBLIC RELEASE, DISTRIBUTION UNLIMITED

TI - ALEX(01)-TR-76-06

ADA 041225

DEVELOPMENT OF THREE SIGNAL PROCESSING TECHNIQUES

2

TECHNICAL REPORT NO.6

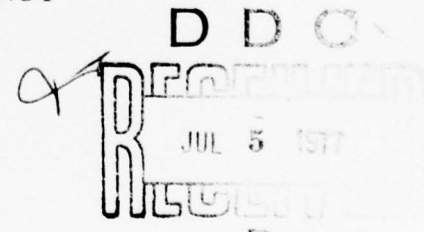
VELA NETWORK EVALUATION AND AUTOMATIC PROCESSING RESEARCH

Prepared by
Stephen S. Lane

TEXAS INSTRUMENTS INCORPORATED
Equipment Group
Post Office Box 6015
Dallas, Texas 75222

Prepared for
AIR FORCE TECHNICAL APPLICATIONS CENTER
Alexandria, Virginia 22314

Sponsored by
ADVANCED RESEARCH PROJECTS AGENCY
Nuclear Monitoring Research Office
ARPA Program Code No. 6F10
ARPA Order No. 2551



29 October 1976

AD No. _____
DDC FILE COPY

Acknowledgment: This research was supported by the Advanced Research Projects Agency, Nuclear Monitoring Research Office, under Project VELA-UNIFORM, and accomplished under the technical direction of the Air Force Technical Applications Center under Contract Number F08606-76-C-0011.

DISTRIBUTION STATEMENT A
Approved for public release;
Distribution Unlimited

Equipment Group

APPROVED FOR PUBLIC RELEASE, DISTRIBUTION UNLIMITED

(14) TI-ALEX(01)-TR-76-06

TR-6

6
DEVELOPMENT OF THREE SIGNAL PROCESSING TECHNIQUES.

TECHNICAL REPORT NO.6

VELA NETWORK EVALUATION AND AUTOMATIC PROCESSING RESEARCH.

(16) Prepared by
Stephen S. Lane

(9) Technical rpt.,

TEXAS INSTRUMENTS INCORPORATED
Equipment Group
Post Office Box 6015
Dallas, Texas 75222

Prepared for

AIR FORCE TECHNICAL APPLICATIONS CENTER
Alexandria, Virginia 22314

ACCESSION FOR	
RTIS	White Section <input checked="" type="checkbox"/>
RCC	Buff Section <input type="checkbox"/>
UNARMED	<input type="checkbox"/>
JUSTIFICATION	<input type="checkbox"/>
BY	
REF IDLE/AVAILABILITY CODES	
DATE RECEIVED	

Sponsored by

ADVANCED RESEARCH PROJECTS AGENCY
Nuclear Monitoring Research Office
ARPA Program Code No. 6F10
ARPA Order 2551

(15) F08606-76-C-0011

(11) 29 Oct 1976

(12) 54P.

D D C
D D P
JUL 5 1976
LUG 1976

Acknowledgment: This research was supported by the Advanced Research Projects Agency, Nuclear Monitoring Research Office, under Project VELA-UNIFORM, and accomplished under the technical direction of the Air Force Technical Applications Center under Contract Number F08606-76-C-0011.

405 076 Equipment Group

UNCLASSIFIED

SECURITY CLASSIFICATION OF THIS PAGE (When Data Entered)

UNCLASSIFIED

SECURITY CLASSIFICATION OF THIS PAGE(When Data Entered)

20. continued

cont.

A representative southern Kamchatka earthquake seismogram was formed by averaging spectra of events from that region. The Wiener filter used the resulting average power spectrum but no signal-noise correlation terms to achieve a 3 to 6 dB maximum gain over the bandpass filter. The average event was also used as a matched filter, which had a gain of 6 to 10 dB over the bandpass filter. With the help of a Monte Carlo simulation to determine the best form for the filter weights, the three component adaptive filter had a gain of from 10 to 17 dB over the bandpass filter.

R

UNCLASSIFIED

SECURITY CLASSIFICATION OF THIS PAGE(When Data Entered)

ABSTRACT

The gain in signal-to-noise ratio with respect to a bandpass filter was investigated as a function of input signal-to-noise ratio for a Wiener filter, a matched filter, and the three component adaptive filter. Each processor was applied to two southern Kamchatka events recorded at a single site at the Alaskan Long Period Array (ALPA) and buried in two noise samples recorded there.

A representative southern Kamchatka earthquake seismogram was formed by averaging spectra of events from that region. The Wiener filter used the resulting average power spectrum but no signal-noise correlation terms to achieve a 3 to 6 dB maximum gain over the bandpass filter. The average event was also used as a matched filter, which had a gain of from 6 to 10 dB over the bandpass filter. With the help of a Monte Carlo simulation to determine the best form for the filter weights, the three component adaptive filter had a gain of from 10 to 17 dB over the bandpass filter.

Neither the Advanced Research Projects Agency nor the Air Force Technical Applications Center will be responsible for information contained herein which has been supplied by other organizations or contractors, and this document is subject to later revision as may be necessary. The views and conclusions presented are those of the authors and should not be interpreted as necessarily representing the official policies, either expressed or implied, of the Advanced Research Projects Agency, the Air Force Technical Applications Center, or the US Government.

TABLE OF CONTENTS

SECTION	TITLE	PAGE
	ABSTRACT	iii
I.	INTRODUCTION	I-1
II.	WIENER FILTER	II-1
III.	MATCHED FILTER	III-1
IV.	THREE COMPONENT ADAPTIVE FILTER	IV-1
V.	CONCLUSIONS	V-1
VI.	REFERENCES	VI-1

LIST OF FIGURES

FIGURE	TITLE	PAGE
I-1	EVENTS SKA+062+02 AL AND KAM-231-19 AL	I-4
I-2	SCHEMATIC GAIN VERSUS INPUT SNR	I-5
II-1	POWER SPECTRA FOR SYNTHETIC EVENT	II-4
II-2	PHASE SPECTRA FOR SYNTHETIC EVENT	II-5
II-3	AVERAGE SOUTH KAMCHATKA SIGNAL	II-6
II-4	ϕ_{pp} , ϕ_{ss} , AND $ \phi_{sp} $ FOR TRANSVERSE COMPONENT OF REFERENCE EVENT AT SNR = 10 dB	II-8
II-5	WIENER FILTER WITHOUT (a) AND WITH (b) SIGNAL-NOISE CORRELATION	II-9
II-6	GAIN VERSUS INPUT SNR FOR WIENER FILTER WITH CONSTANT SIGNAL	II-11
II-7	GAIN VERSUS INPUT SNR FOR WIENER FILTER WITH CONSTANT NOISE	II-12
II-8	OUTPUT WAVEFORMS FOR SNR OF 12 dB FOR WIENER FILTER (KAM-231-19 AL IN NOI-311-08 AL)	II-14
II-9	OUTPUT WAVEFORMS FOR SNR OF 12 dB FOR BANDPASS FILTER (KAM-231-19 AL IN NOI-311-08 AL)	II-15
III-1	GAIN VERSUS INPUT SNR FOR MATCHED FILTER WITH CONSTANT SIGNAL	III-3
III-2	GAIN VERSUS INPUT SNR FOR MATCHED FILTER WITH CONSTANT NOISE	III-4
III-3	MATCHED FILTER OUTPUTS (KAM-231-19 AL IN NOI-311-08 AL)	III-6
IV-1	LOVE WAVE FILTER DESIGN	IV-3
IV-2	PROBABILITY DISTRIBUTION FUNCTIONS FOR β	IV-5

LIST OF FIGURES
(continued)

FIGURE	TITLE	PAGE
IV-3	TCA WEIGHTING FUNCTION	IV-6
IV-4	RAYLEIGH WAVE FILTER DESIGN	IV-7
IV-5	PROBABILITY DISTRIBUTION FUNCTIONS FOR ψ	IV-9
IV-6	GAIN VERSUS INPUT SNR FOR TCA WITH CONSTANT SIGNAL	IV-10
IV-7	GAIN VERSUS INPUT SNR FOR TCA WITH CONSTANT NOISE	IV-11
IV-8	TCA OUTPUTS (KAM-231-19AL IN NOI-311-08AL)	IV-12

LIST OF TABLES

TABLE	TITLE	PAGE
I-1	EVENTS AND NOISE SAMPLES	I-3

SECTION I INTRODUCTION

This report describes the performance of three important processors for seismic data: the Wiener filter, the matched filter, and the three component adaptive (TCA) processor. Each has been optimized as far as possible for the present application.

The data used here were single-site Alaskan Long Period Array (ALPA) signals and noise samples. Single-site data were used because the detection problem is more severe for a single instrument than for an array, and because the trend at present is toward deployment of single-site instrumentation (Seismic Research Observatories) and small arrays (Iranian Long Period Array). ALPA data were used because they are of high quality and because the nature of noise and signals at ALPA is well known.

Synthetic data were prepared by selecting a 2048-point segment of seismic noise, sampled every two seconds, and adding to it a suitably scaled signal, originally recorded at high signal-to-noise ratio (SNR), to form a composite trace. The ratio of the scaled signal peak to the root-mean-square (RMS) value of the noise preceding the time at which the signal was added was the true input signal-to-noise ratio. For the matched and Wiener filters, different scale factors were used for each trace so that all had the same SNR. For the TCA, a common scale factor was used so that the signal was not distorted. This procedure has the advantage over use of signals as recorded that the true SNR and peak arrival time are known exactly, and can be varied by the experimenter.

The signal buried in noise is called the test event. Another event is required for implementation of the Wiener and matched filter and is

called the reference event. Descriptions of the noise samples and test events used in this study are given in Table I-1, and the events are plotted in Figure I-1.

The general experimental procedure was as follows. The test event was buried in noise at various known SNR's, and the processor under study applied to the composite trace. The ratio of the largest peak in the signal arrival interval to the RMS value of the preceding noise was calculated. The SNR was also calculated for the same composite trace filtered between 0.024 Hz and 0.059 Hz, the frequency range where the SNR of seismic events is expected to be large. The difference (in dB) between these ratios was the gain of the processor over the bandpass filter and was plotted as a function of input SNR.

It is useful to present gains rather than absolute SNR's because gains do not increase indefinitely with input SNR, but saturate at some maximum value. The bandpass filter was chosen as a standard because it is a routine form of signal improvement whose performance is well known.

A schematic form for the results is shown in Figure I-2. The horizontal axis is input SNR and the vertical axis is SNR gain over the bandpass filter. Both scales are in dB, although no values are shown.

At low values of input SNR the signal is so far below the noise that the peak of the processor output is not contributed by the signal. Consequently, the gain is not a function of the input SNR. At sufficient input SNR, the processor output is determined by the signal, although, hopefully, the bandpass filters' output is still due to noise. At this point the gain of the processor begins to increase. At some higher SNR the bandpass filter peak is due to the signal, and thereafter little gain is obtained. In some cases the gain may decrease. In any case, the SNR gain reaches a maximum, as shown in Figure I-2, and this maximum gain is taken here as a measure of processor performance.

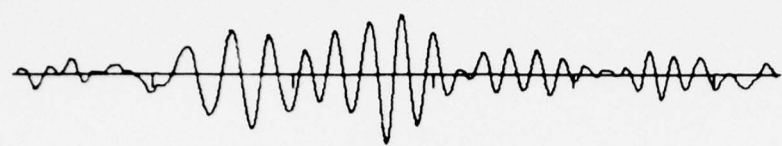
TABLE I-1
EVENTS AND NOISE SAMPLES

Event	Date	Origin Time	Location	m_b
KAM-231-19AL	08/18/72	19:02:01	53.0N 159.9E	5.1
SKA+062+02 AL	03/03/73	02:42:09	50.4N 156.2E	5.5

Noise Sample	Date	Start Time
NOI-041-22AL	02/10/72	22:00:00
NOI-311-08AL	11/06/72	08:40:00

SKA+062+02 AL

Vertical



Transverse

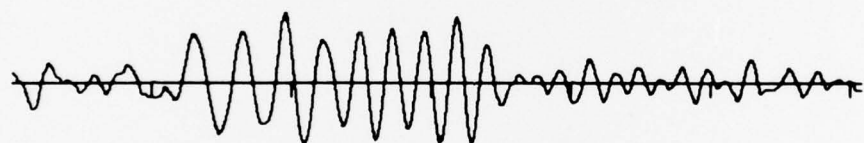


Radial

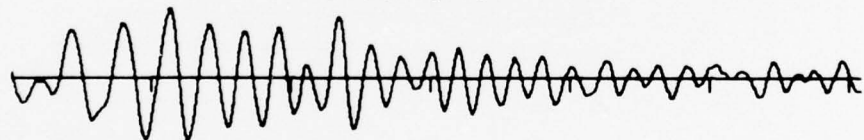


KAM-231-19AL

Vertical



Transverse



Radial

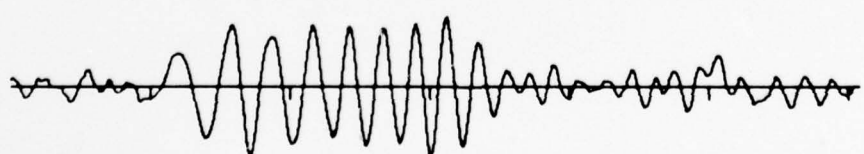


FIGURE I-1

EVENTS SKA+062+02 AL AND KAM-231-19AL

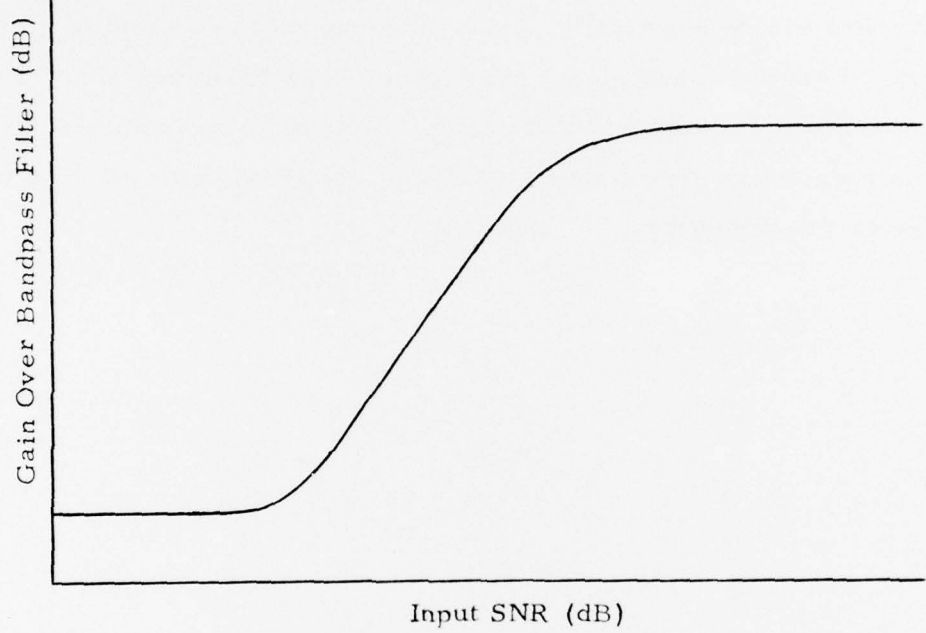


FIGURE I-2
SCHEMATIC GAIN VERSUS INPUT SNR

The curves presented here are not as regular as implied by the preceding paragraphs, in that they may display kinks, ill-defined shoulders, or occasionally no shoulders at all. Since the exact behavior of both signal and noise are known in a study such as this, each unusual feature could be explained by a detailed examination of the data and the processor. Such an explanation is not attempted because, while the basic process giving rise to signal and noise are deterministic, from the geophysicist's point of view they are random. Both noise and signal are thought of as being drawn from some population, and are unlikely to occur again. Thus only the most general features of the results are repeatable, and deviations from them must be expected and treated as fluctuations.

SECTION II
WIENER FILTER

The Wiener filter is one whose output is closest to the desired signal in the least mean square sense. In the frequency domain, it takes the following form:

$$F = \frac{\phi_{ss} + \phi_{sn}}{\phi_{ss} + \phi_{sn} + \phi_{ns} + \phi_{nn}} \quad (\text{II-1})$$

where the ϕ 's are the cross- and auto-power spectra of the signal and noise. Thus, if x is the test event which it is desired to extract from the noise sample z , the ϕ 's are defined as follows:

$$\phi_{nn} = \tilde{z}(\omega) \cdot \tilde{z}^*(\omega) \quad (\text{II-2})$$

$$\phi_{sn} = \tilde{x}(\omega) \cdot \tilde{z}^*(\omega) \quad (\text{II-3})$$

$$\phi_{ns} = \tilde{x}(\omega) \cdot \tilde{z}^*(\omega) \quad (\text{II-4})$$

$$\phi_{ss} = \tilde{x}(\omega) \cdot \tilde{x}^*(\omega) \quad (\text{II-5})$$

where ω is the angular frequency, the symbol \sim denotes a Fourier transform, and $*$ denotes a complex conjugate.

The Wiener filter in the form of equation (II-1) is in a sense trivial. Rewriting it using equations (II-2) through (II-5), we have the following:

$$F = \frac{\tilde{x}(\omega)\tilde{x}^*(\omega) + \tilde{x}(\omega)\tilde{z}^*(\omega)}{\tilde{x}(\omega)\tilde{x}^*(\omega) + \tilde{x}(\omega)\tilde{z}^*(\omega) + \tilde{z}(\omega)\tilde{x}^*(\omega) + \tilde{z}(\omega)\tilde{z}^*(\omega)} . \quad (\text{II-6})$$

The denominator of equation (II-6) can be factored as can the numerator, as follows:

$$F = \frac{\tilde{x}(\omega) (\tilde{x}(\omega) + \tilde{z}(\omega))^*}{(\tilde{x}(\omega) + \tilde{z}(\omega)) (\tilde{x}(\omega) + \tilde{z}(\omega))^*} . \quad (II-7)$$

The output of the filter is F times the input $\tilde{x}(\omega) + \tilde{z}(\omega)$, and is:

$$F \{ \tilde{x}(\omega) + \tilde{z}(\omega) \} = \frac{\tilde{x}(\omega) (\tilde{x}(\omega) + \tilde{z}(\omega))^*}{(\tilde{x}(\omega) + \tilde{z}(\omega)) (\tilde{x}(\omega) + \tilde{z}(\omega))^*} \{ \tilde{x}(\omega) + \tilde{z}(\omega) \} = \tilde{x}(\omega) . \quad (II-8)$$

This result means that if the signal and noise are known exactly, the signal can be extracted exactly from the noise. The utility of the Wiener filter is, of course, that the form of equation (II-1) can also be used when signal and noise are only approximately known.

The problem, then, is to estimate the terms in equation (II-1). The noise power spectrum ϕ_{nn} can be found from the noise preceding the signal arrival, and, as usual, we will assume that the noise is stationary so that this power spectrum can be used to estimate the power spectrum in the presence of the signal. A model for the signal must be assumed in order to calculate ϕ_{ss} . A model is also required to find the crosspower terms ϕ_{sn} , and no satisfactory way of doing this has been found.

The noise power spectrum was estimated by segmenting a 2048-point series into 8 sections of 256 points each, filling with zeros to make 2048 points, and Fourier transforming. At each frequency, the power was the sum of the squares of the real and imaginary parts. These powers were averaged at each frequency over all 8 segments to increase the reliability of the estimates.

The signal power spectrum was found by averaging power spectra from seven southern Kamchatka events together. Each had been normalized

to unit area before averaging, to eliminate the influence of magnitude. The average power spectra are shown in Figure II-1.

Phase spectra for these events were corrected for jumps of 2π by adding or subtracting 2π whenever such a jump was found. Then their linear trend was removed by subtracting the quantity $(f/f_n)\psi_n$ from the phase angle at frequency f , where f_n is the Nyquist frequency and ψ_n was the phase at the Nyquist frequency of the transverse component. This had the effect of moving each signal without distortion so that it was centered on zero time.

Finally, the seven corrected phase spectra were averaged together for each component and are shown in Figure II-2. In regions where the signal power is low, the phase spectrum is meaningless, but over the signal band the slope of the phase spectrum is indicative of the phase velocity of the signal.

An amplitude spectrum was calculated for each component by extracting the square root of the power spectrum, and the inverse transform of this amplitude and phase spectrum found and plotted in Figure II-3. These synthetic signals show the effects of multipathing (which is also visible in the scalloping of the power spectra in Figure II-1), of dispersion, and of the higher group velocity of Love waves than Rayleigh waves. This time-domain signal will also be used as a matched filter, and is denoted as $s(t)$.

The average correlation coefficient between the synthetic signal found here and seven independent events from southern Kamchatka was 0.69, with a standard deviation of 0.08. The average correlation between KAM-231-19AL and the same seven events was 0.64, with a standard deviation of 0.18. These mean correlations are indistinguishable, but the standard deviation for the synthetic signal is less than for the real one. This means that although there is no advantage in terms of gain in using the

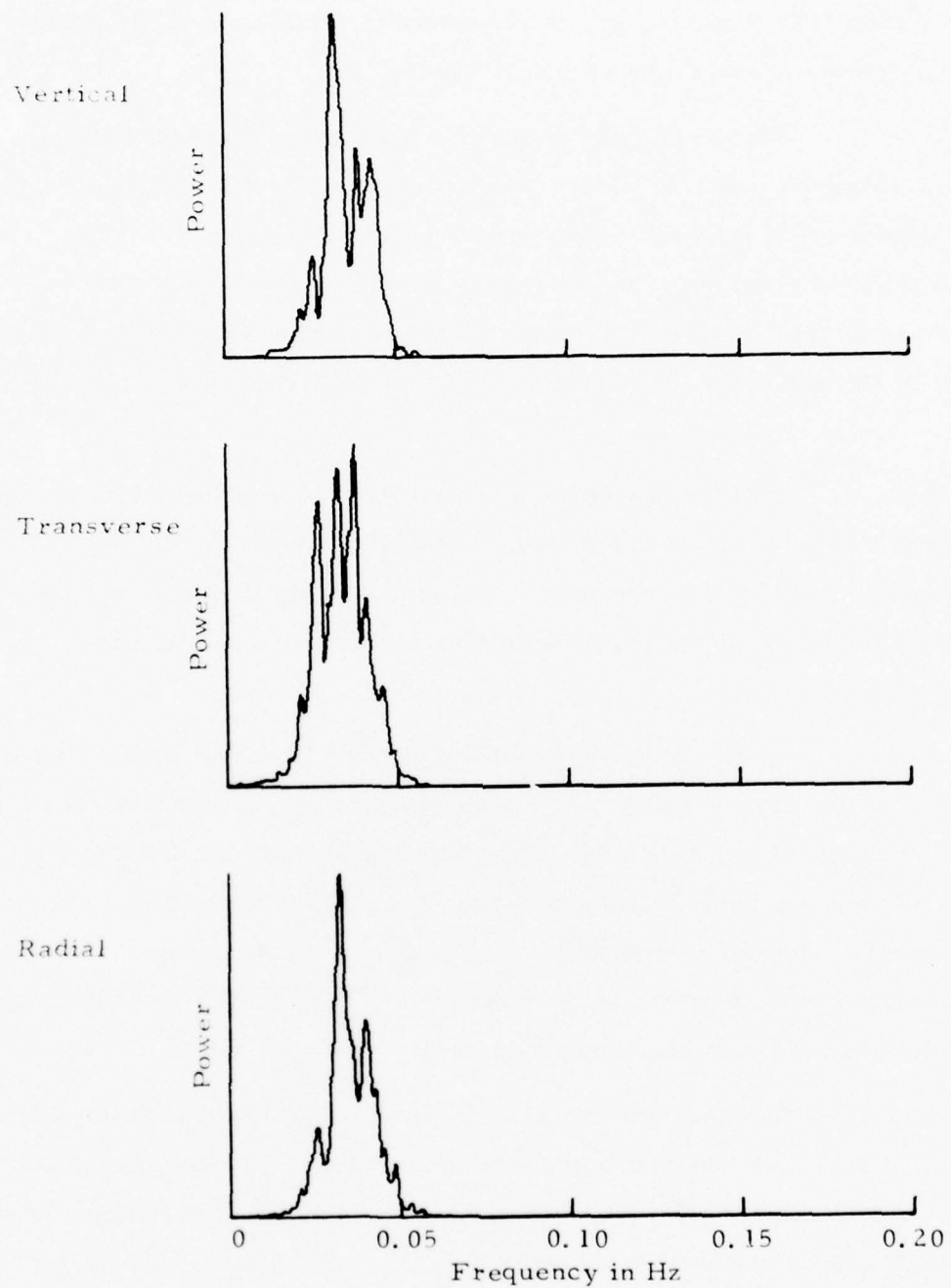


FIGURE II-1
POWER SPECTRA FOR SYNTHETIC EVENT

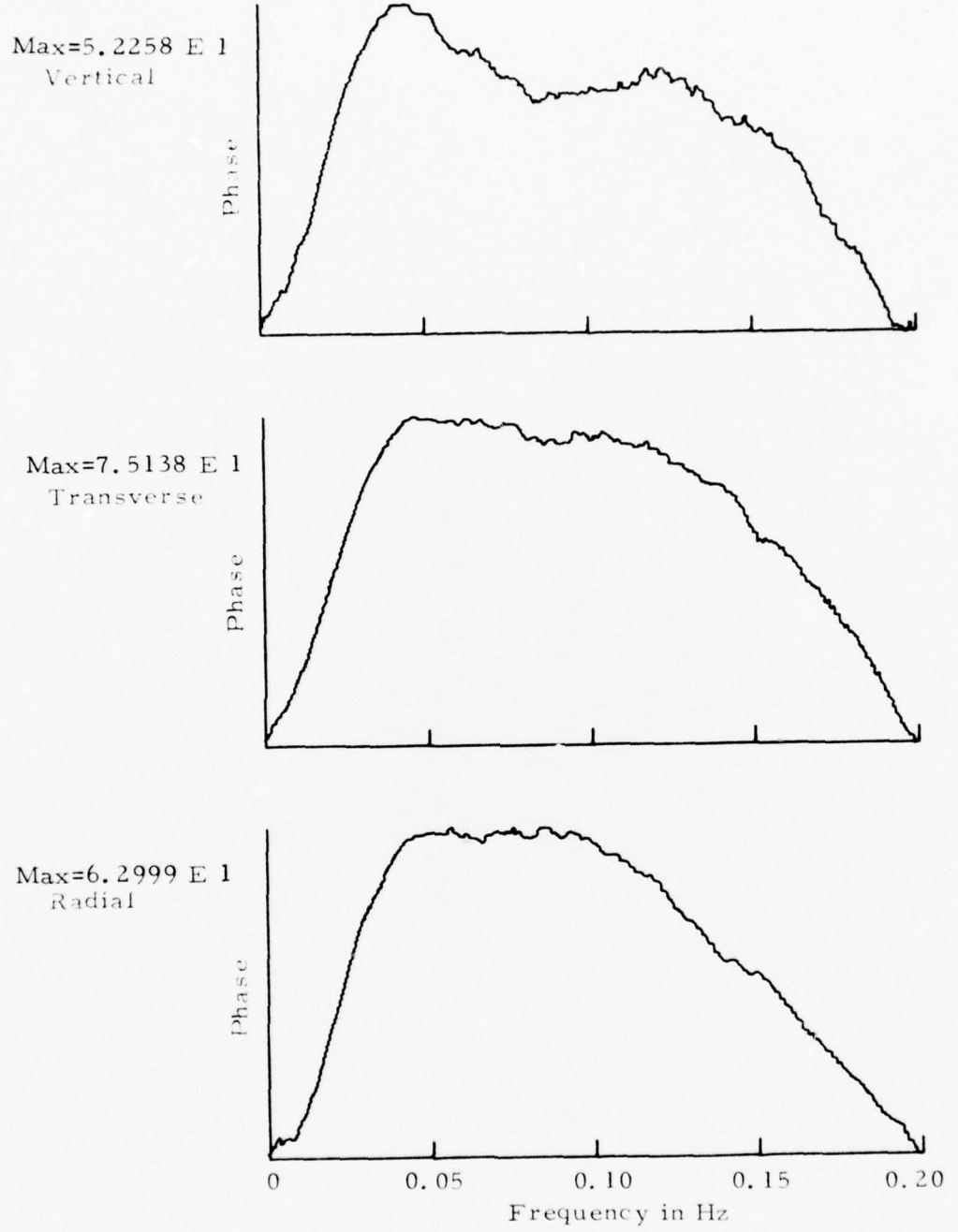


FIGURE II-2
PHASE SPECTRA FOR SYNTHETIC EVENT

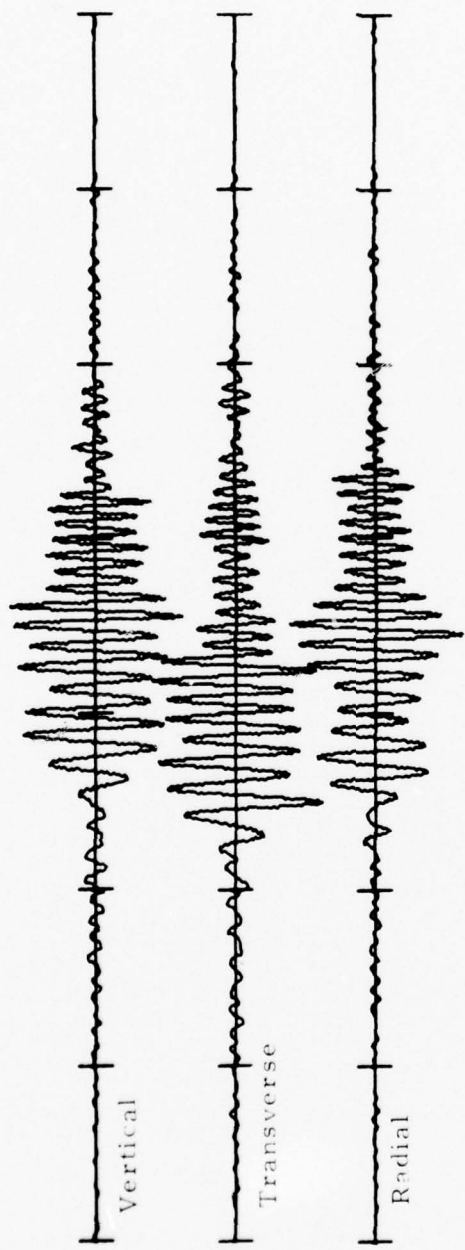


FIGURE II-3
AVERAGE SOUTH KAMCHATKA SIGNAL

synthetic waveform, there is a higher likelihood of detecting a signal using the synthetic waveform, since detection is a yes-no decision depending on a threshold.

The assumption is ordinarily made that signal and noise are uncorrelated so that terms like ϕ_{sn} may be ignored. While this is true on the average, over the short sections of data used here there will be some apparent correlation between signal and noise due to the random nature of the noise. Furthermore, at low enough values of signal-to-noise ratio, the correlation term ϕ_{sn} will dominate the numerator of equation (II-1), since it is proportional to the first power of the signal amplitude, while ϕ_{ss} is proportional to the square of the signal amplitude. Consequently, it is important to include ϕ_{sn} in the Wiener filter.

The terms contributing to the Wiener filter for the transverse component are plotted in Figure II-4. Here a signal-to-noise ratio of 10 dB has been used, and ϕ_{ss} , ϕ_{nn} , and $|\phi_{sn}|$ plotted on the same scale as a function of frequency. Since the phase angle of the noise is random, the phase of ϕ_{sn} is also random, and is not shown.

The influence of the signal-noise correlation terms is shown explicitly in Figure II-5, where the Wiener filter is shown for the same signal and noise, at 10 dB signal-to-noise ratio, with and without the correlation terms. For comparison, the bandpass filter used here is also shown. It is clear that their inclusion makes a significant difference to the filter weights. The term ϕ_{sn} in the numerator also introduces a phase shift into the filter.

Having established the importance of the signal-noise correlation terms, the next step is to calculate them for an unknown signal. The average amplitude of ϕ_{sn} is easy enough to find, but its phase is unpredictable, since the noise phase is a random variable depending on the details of the time domain motion, and can take on with equal probability any value over

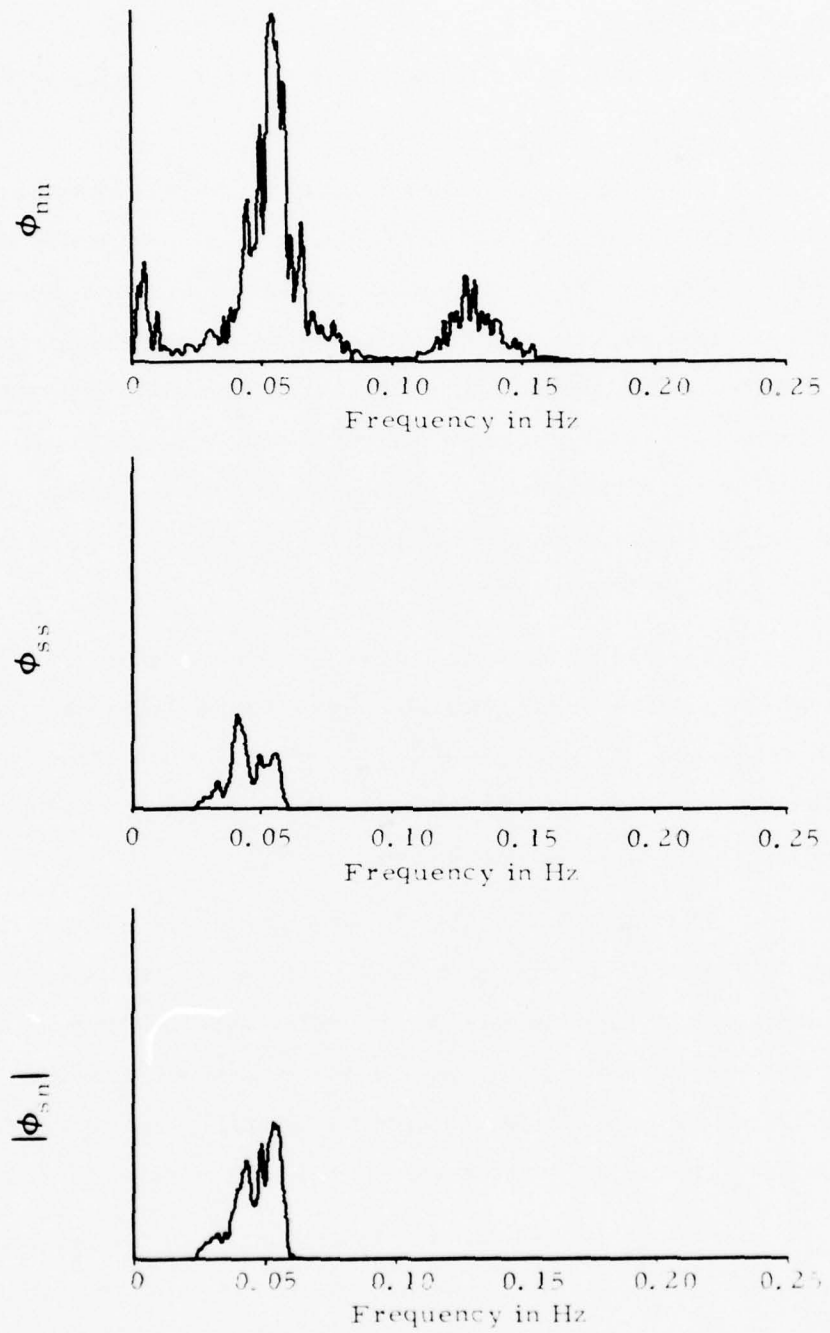
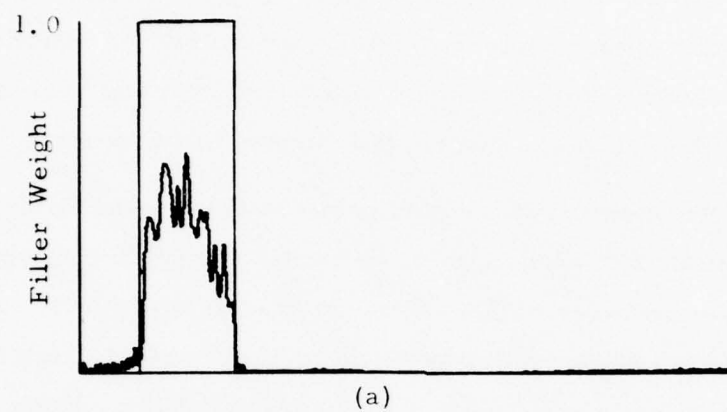
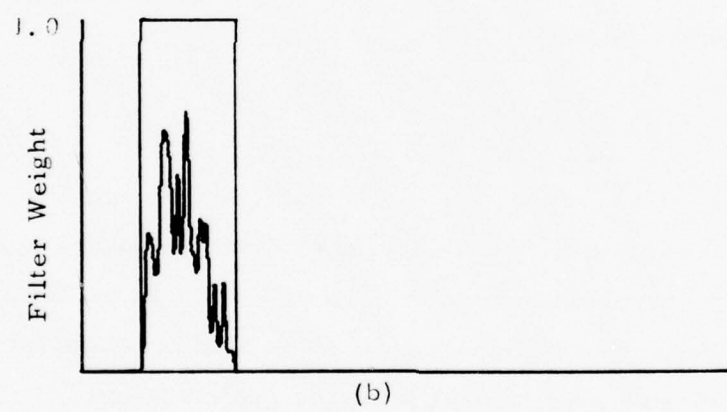


FIGURE II-4
 Φ_{nn} , Φ_{ss} , AND $|\Phi_{sn}|$ FOR TRANSVERSE COMPONENT
 OF REFERENCE EVENT AT SNR = 10 dB



(a)



(b)

FIGURE II-5
WIENER FILTER WITHOUT (a) AND WITH
(b) SIGNAL-NOISE CORRELATION

its whole range. The probability distribution function of the power, by contrast, is peaked at the mean power, so that the power at a given frequency is much more predictable than the phase. There are many time series having the same power spectrum but different phase spectra, and these time series differ in that their energy appears at different times. In practice, this randomness in the distribution of energy in the time domain, and the resulting randomness of the phase spectrum, was impossible to model.

To examine the performance of the Wiener filter, it was calculated for a number of signal-to-noise ratios and applied to signals buried at the appropriate level in noise. Various models of the noise phase were examined. The noise phase was taken to be its expected value of zero, or to be a random number, or to be equal to the signal phase. None of these choices was as effective as omitting the correlation term entirely. Consequently, all results for the Wiener filter presented here assume that $\phi_{sn} = 0$. The filter weights are then as follows:

$$F = \frac{\phi_{ss}}{\phi_{ss} + \phi_{nn}} . \quad (\text{II-9})$$

The gain of the Wiener filter over the bandpass filter is shown as a function of input SNR in Figures II-6 and II-7. In the first figure, the noise sample is varied while the test event is held constant, and the opposite is true in Figure II-7. More correlation is seen between results with a common test event than those with a common noise sample, because the performance of the filter is principally affected by the correlation between test and reference events rather than by the uniformly low correlation between the noise and reference event.

Gains are rather low compared to those from other processors studied here. Peak gains varied from 2 to 6 dB and occurred at from 6 to 16

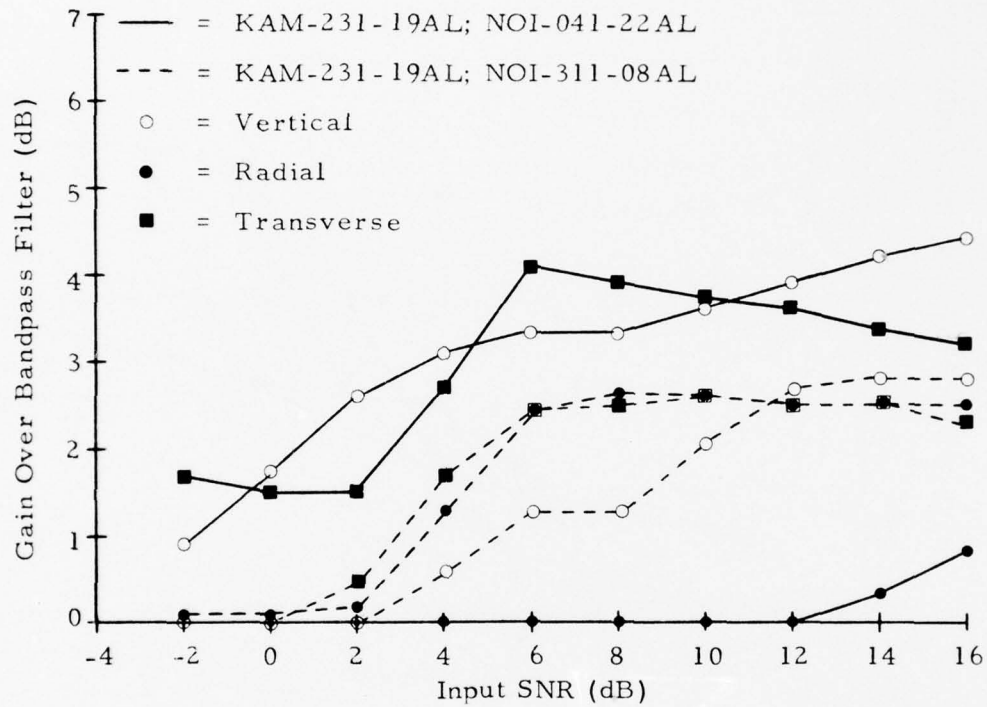


FIGURE II-6
GAIN VERSUS INPUT SNR FOR
WIENER FILTER WITH CONSTANT SIGNAL

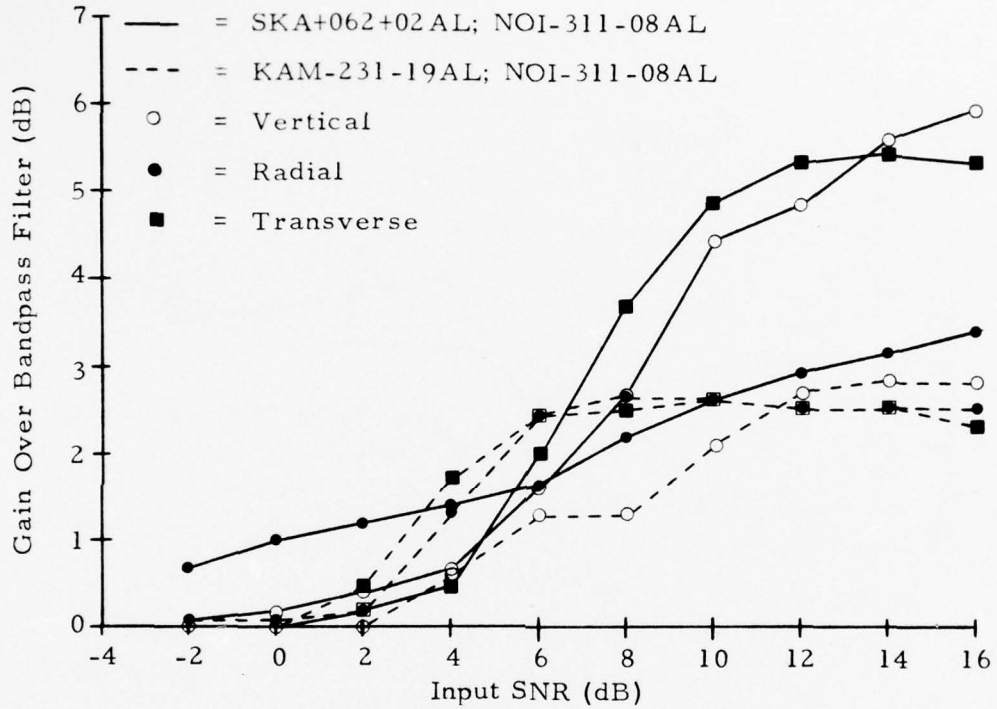


FIGURE II-7
GAIN VERSUS INPUT SNR FOR
WIENER FILTER WITH CONSTANT NOISE

dB input SNR. Output waveforms for an input SNR of 10 dB are shown for the Wiener filter in Figure II-8 and for the bandpass filter in Figure II-9, for KAM-231-19AL buried in noise sample NOI-311-08AL.

Without the signal-noise correlation terms the Wiener filter is just a zero-phase filter with a shape which suppresses more of the noise (and of the signal) than does the simple rectangular bandpass filter. Since no qualitatively different operations are performed, it is not surprising that the gain over the bandpass filter should not be large. We may also conclude from the small changes in performance when the noise sample was changed that the noise and signal spectral peaks are fairly well separated, at least for that signal.

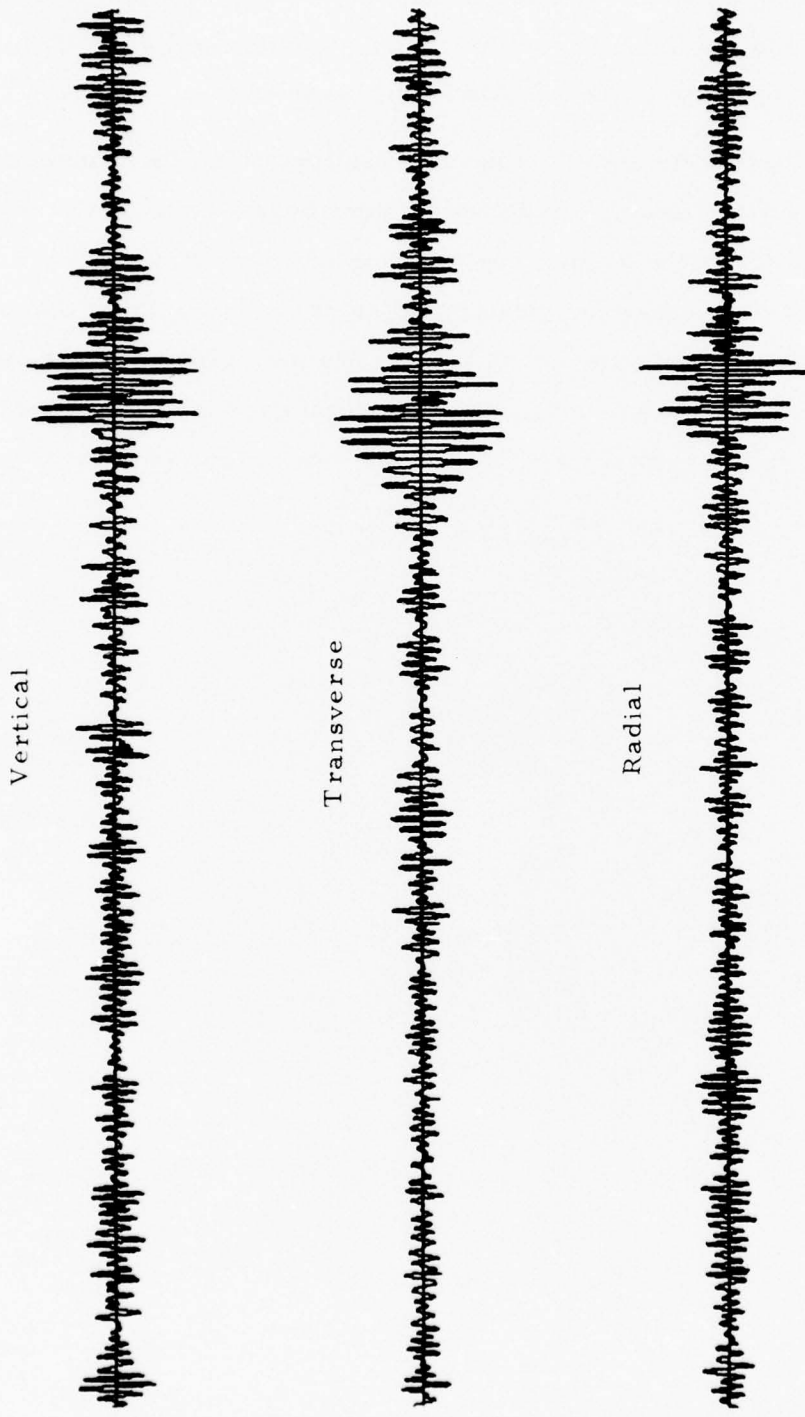
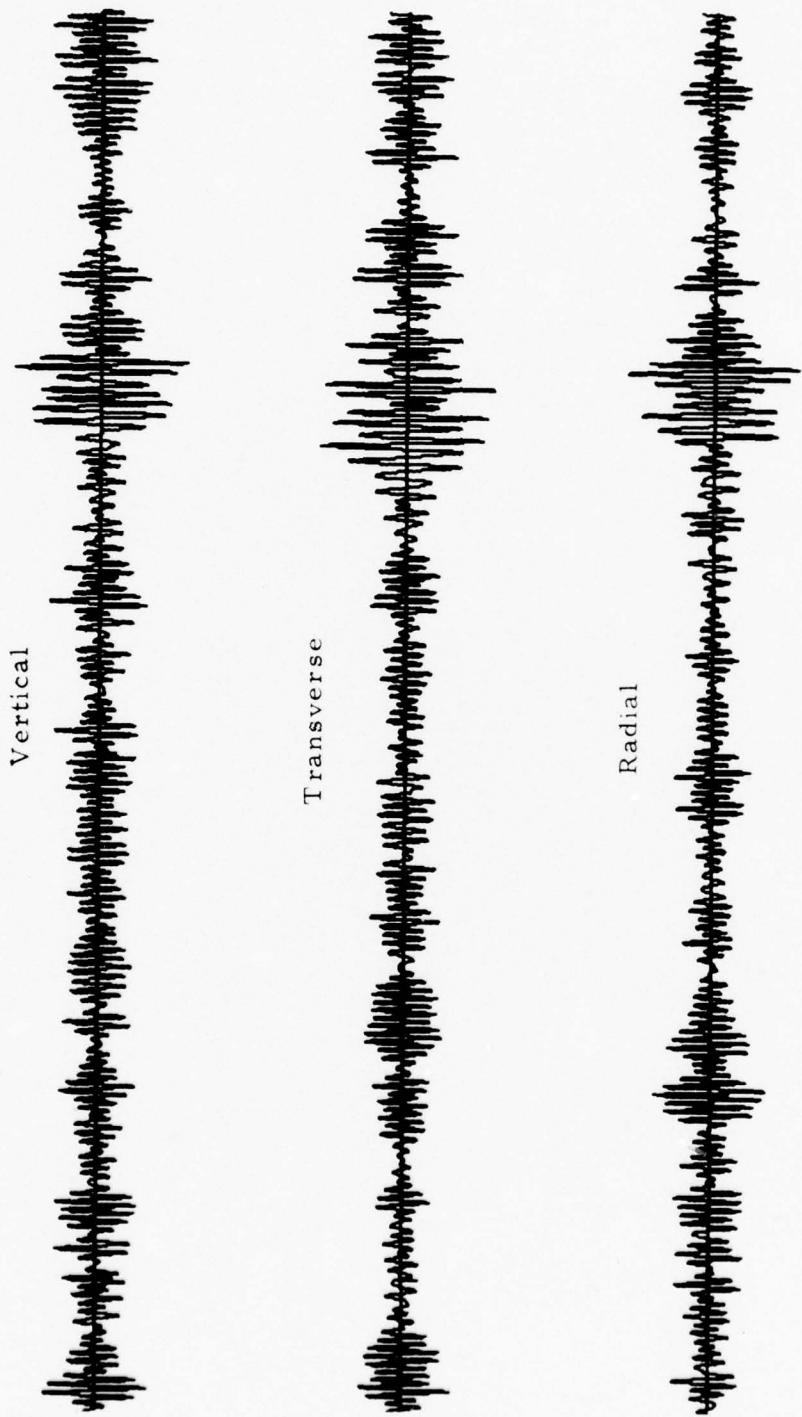


FIGURE II-8
OUTPUT WAVEFORMS FOR SNR OF 10 dB FOR WIENER FILTER
(KAM-231-19AL IN NOI-311-08AL)



II-15

FIGURE II-9
OUTPUT WAVEFORMS FOR SNR OF 10 dB FOR BANDPASS FILTER
(KAM-231-19AL IN NOI-311-08AL)

SECTION III MATCHED FILTER

Prewhitenning followed by matched filtering is the optimum detection scheme (Capon, Greenfield, and Lacoss, 1969). Prewhitenning is accomplished by dividing the transform of the trace to be processed by the power spectrum $p(\omega)$ of the noise. The matched filter used here is the synthetic signal developed in the previous section on Wiener filtering, and is convolved with the prewhitened input trace to yield an output \tilde{y} .

Using the notation of the previous section, where $x(t)$ is the test event, $z(t)$ the noise, and $s(t)$ the matched filter waveform, the operations of matched filtering and prewhitening can be combined into one expression in the frequency domain, as follows:

$$\tilde{y} = \frac{\{x(\omega) + z(\omega)\} s^*(\omega)}{p(\omega)} . \quad (\text{III-1})$$

Comparing this expression to that for the Wiener filter without crosscorrelation terms (equation (II-9)), it is evident that the Wiener filter output is approximately the prewhitened matched filter output convolved with the reference waveform. Intuitively, it would seem that such convolution can only reduce the signal-to-noise ratio and that the Wiener filter should display less gain than does the matched filter. It will be seen that this is the case.

The output of the filter (equation (III-1)) is proportional to the input, but with unknown scale factor. In order to find correct peak amplitudes, we calculate a multiplicative scale factor for the reference waveform that will ensure that matched filtering a waveform with itself in the absence of noise

will yield a peak amplitude equal to that of the original signal. This requirement is satisfied if:

$$I \left\{ \frac{g \tilde{s}(\omega) \tilde{s}^*(\omega)}{p(\omega)} \right\}_{\max} = s(t)_{\max} \quad (\text{III-2})$$

where g is the desired scale factor, I denotes inverse Fourier transformation, and the subscript 'max' denotes taking the maximum of a waveform.

Then:

$$g = \frac{s(t)_{\max}}{I \left\{ \frac{\tilde{s}(\omega) \tilde{s}^*(\omega)}{p(\omega)} \right\}_{\max}} . \quad (\text{III-3})$$

The function in the denominator of equation (III-3) is the prewhitened autocorrelation function of the reference waveform.

The scale factor g thus found is not a function of the test event, so that it can be used to extract an unknown event. The matched filter peak will be somewhat smaller than the true value because of less than perfect correlation between test and reference events, but this loss will be only about 3 dB for a correlation of 0.7.

Gains as a function of input SNR are shown in Figures III-1 and III-2 in the same format as in the previous chapter. Figure III-1, for constant signal, shows some similarity in the shape of the gain curves as the noise is varied, as for the Wiener filter, although the levels are different. Again, this is because the gain is determined by the test event-reference event correlation, reference event-noise correlation being uniformly low.

There is no obvious similarity between gains for the same component from different events in Figure III-2, where the noise sample is held constant. This is because the most important factor, the correlation between test and reference event, is not constant. Furthermore, prewhitening removes some of the effect of varying the noise sample.

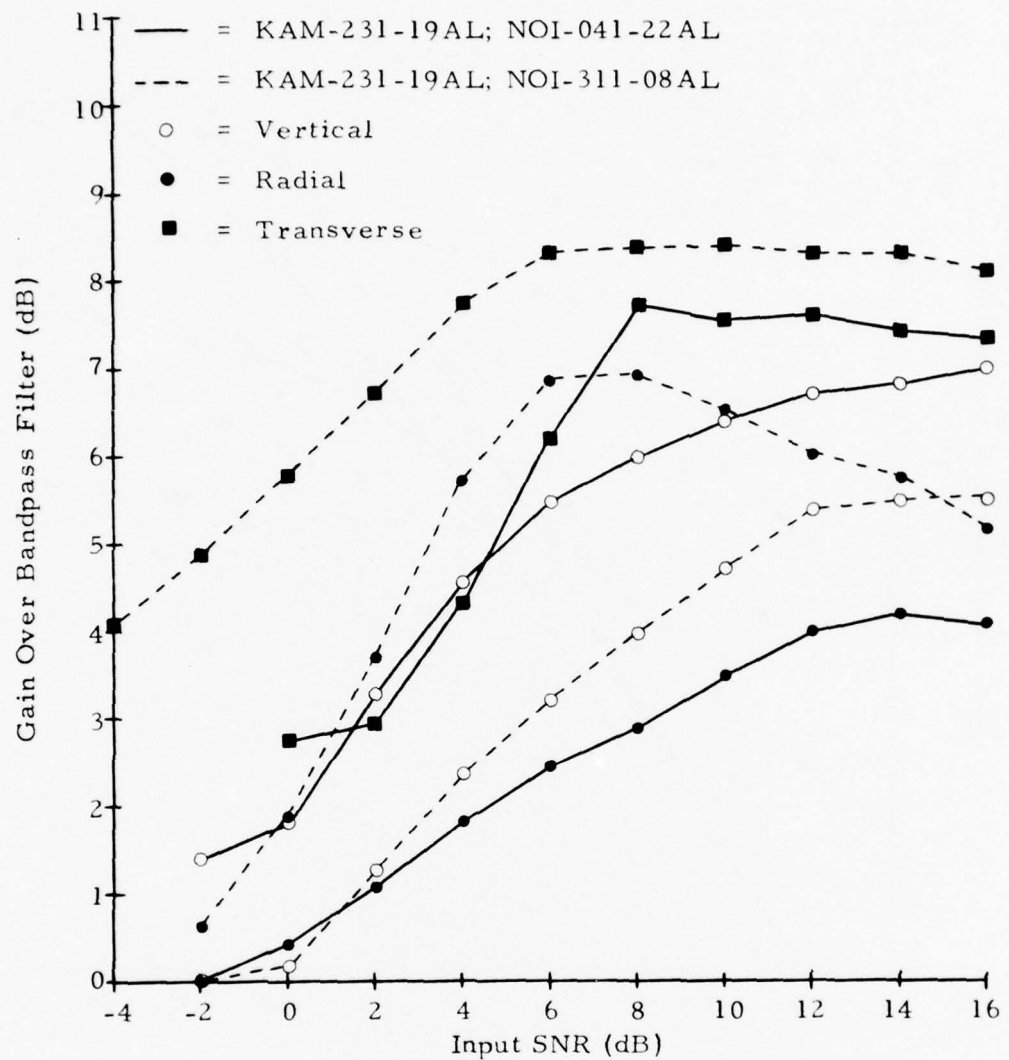


FIGURE III-1
GAIN VERSUS INPUT SNR FOR
MATCHED FILTER WITH CONSTANT SIGNAL

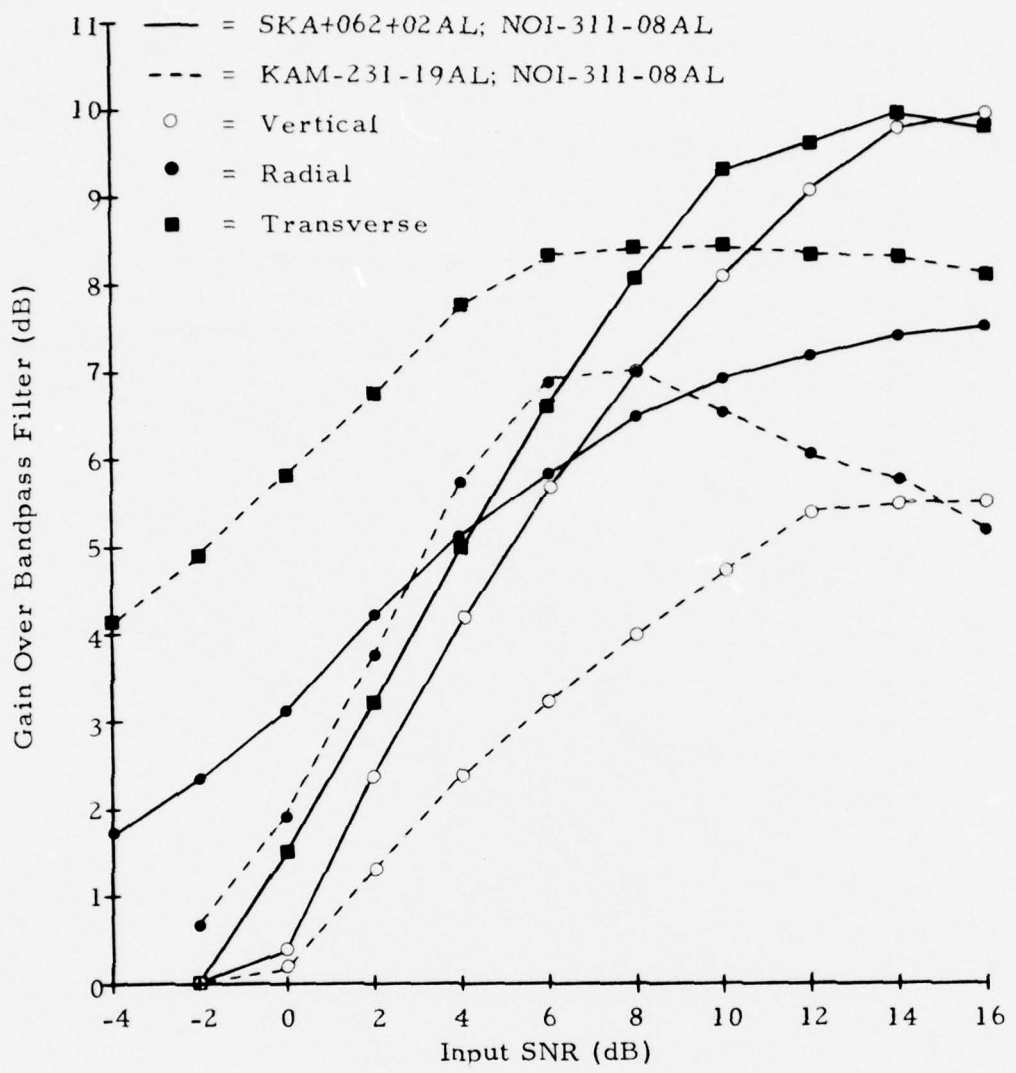


FIGURE III-2
GAIN VERSUS INPUT SNR FOR
MATCHED FILTER WITH CONSTANT NOISE

There is clear similarity between Figures III-1 and III-2 with Figures II-6 and II-7, the corresponding Wiener filter results. The Wiener filter results are roughly parallel to the matched filter results, component by component, but lie about 3 dB below them. This is consistent with the discussion earlier in this chapter where it was pointed out that the Wiener filter output is just the matched filter output convolved with a reference waveform. This process of convolution can now be seen to lose about 3 dB in terms of output SNR.

A plot of matched filter outputs for KAM-231-19AL buried at a true SNR of 10 dB in noise sample NOI-311-08AL is shown in Figure III-3. The peaks occur at the signal arrival time rather than at the peak arrival time as do processors which do not concentrate the signal energy into a single point.

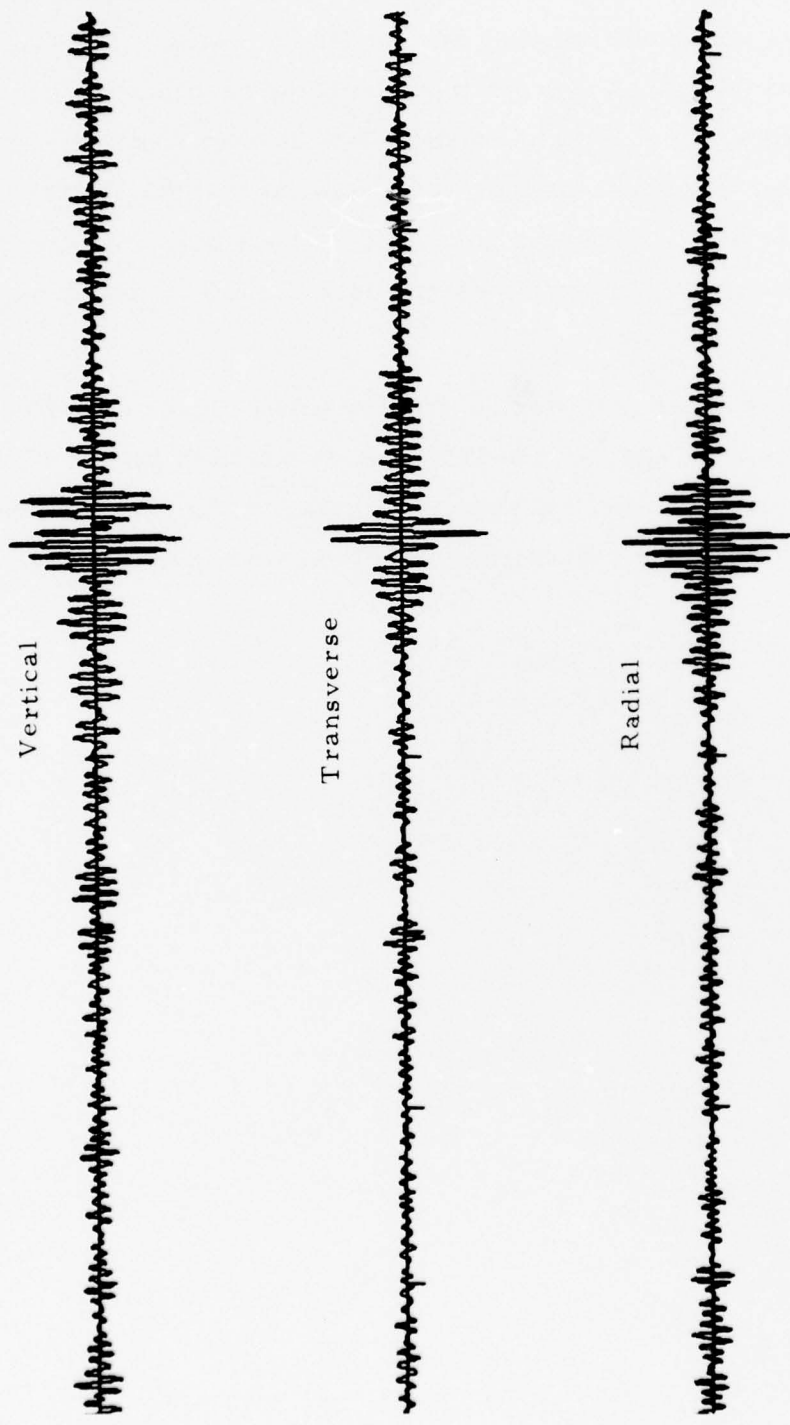


FIGURE III-3
MATCHED FILTER OUTPUTS
(KAM-231-19AL IN NOI-311-08 AL)

SECTION IV

THREE COMPONENT ADAPTIVE FILTER

The three component adaptive filter (TCA) examined here has been described by Strauss (1976). It makes use of all three components of the seismic record simultaneously and designs a data-dependent filter for each of a large number of overlapping segments of the record. The filter applied to the vertical and radial components has large filter weights at frequencies where the phase angle between those components is 90 degrees; i.e., Rayleigh waves only are passed. The transverse filter coefficients are large when transversely-polarized energy is present, so that Love waves are passed. Only energy in phase with the vertical motion is considered in the design of the transverse filter, in order to avoid confusion of Rayleigh waves with off-azimuth Love waves.

The basic design of this filter is fixed, and optimization of its performance can come only through variation of parameters. The parameters examined here were the length of the overlapping data segments, the number of segments overlapped at each time point, and the dependence of the filter weights on the data.

It was found that there was no significant difference in performance when 64 point or 128 point overlapping segments were used, and this result is consistent with previous studies. Some degradation was observed when 32 point and 256 point segments were used, so that a 64 point segment was used in this study in the interest of reduced computational time.

Next, four segments of data were overlapped, rather than only two as in all previous studies. It was hoped that this would result in more

rapid adaptation, due to shorter intervals between initial segment points, but without reduction in frequency resolution due to decreased segment length. However, no difference in performance between this processor and that overlapping only two segments was found, although from 32 to 256 point segments were examined. Therefore, the original version was retained, again in the interest of computational speed.

In both Love and Rayleigh filters, the filter weight is a function of an angle. For the Rayleigh filter the relevant angle is that between the phases of the vertical and radial Fourier components of motion, while for the Love filter it is the angle in space between the horizontal particle motion and the direction of propagation. Since it would be impossible to examine all functional forms for these filter weights, a Monte Carlo method was adopted to find reasonable candidates.

The model used for the Love wave filter design is illustrated in Figure IV-1. An on-azimuth Love wave S_t and noise are present. The noise is assumed to have equal amplitude N in transverse and radial directions and random phase with respect to the vertical Fourier component of motion. Since only motion in phase with the vertical is considered, the effective noise amplitude is its true amplitude multiplied by the cosine of its (random) phase angle γ . The angle β in Figure IV-1 is:

$$\beta = \tan^{-1} \frac{N \cos \gamma_r}{S_t + N \cos \gamma_t} \quad (\text{IV-1})$$

and we desire the distribution of this angle, given that the phase angles of the transverse and radial components of the noise, γ_t and γ_r , are distributed uniformly over the range of 0 to 2π .

This problem would be difficult to solve analytically, but lends itself to the Monte Carlo method. At each signal-to-noise ratio of interest, we choose a large number (say 1000) of pairs of independent numbers γ_t

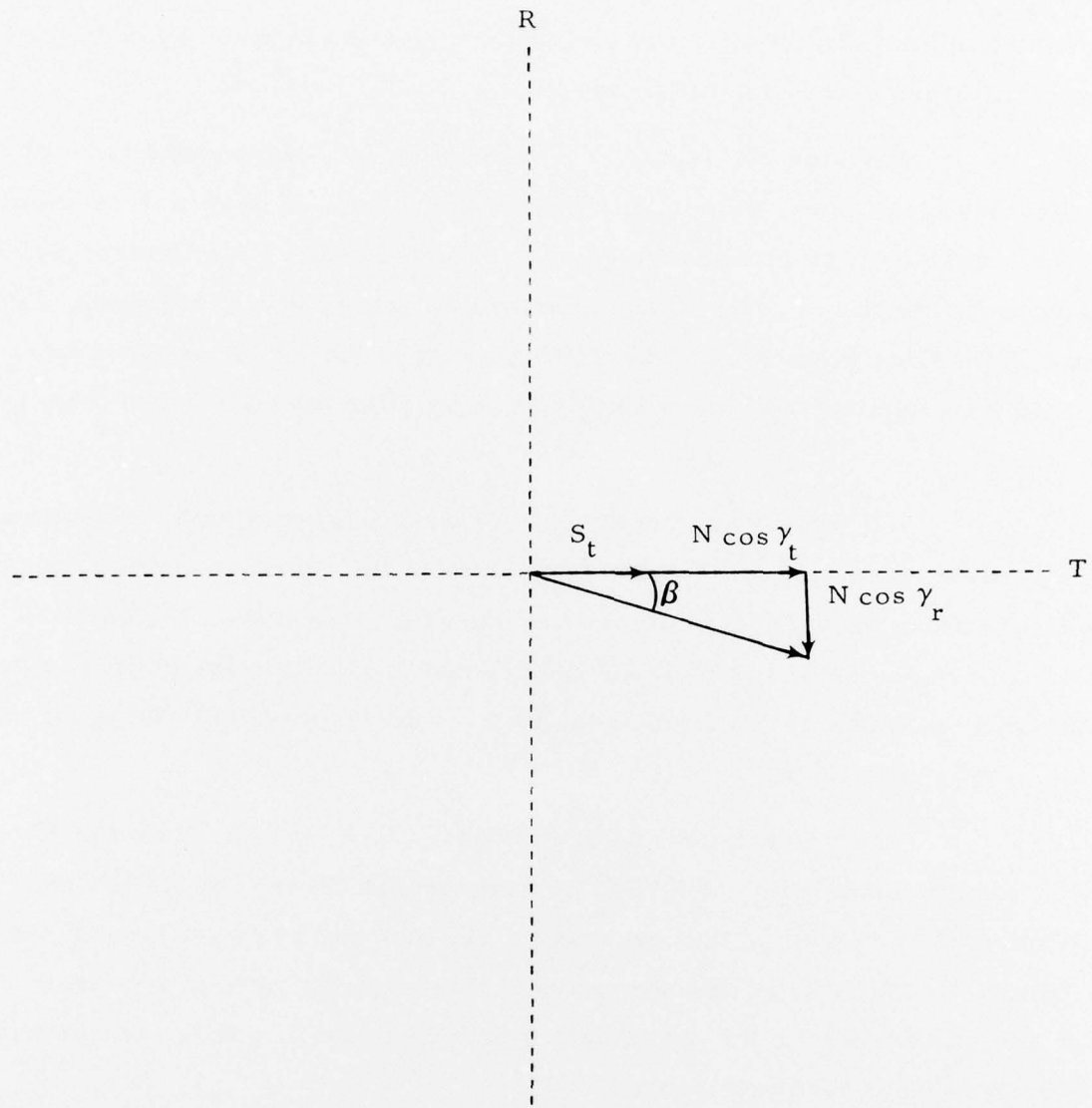


FIGURE IV-1
LOVE WAVE FILTER DESIGN

and γ_r uniformly distributed between 0 and 2π , and compute the corresponding values of β . The probability distribution function is found by counting the number of times each value of β occurs.

The signal-to-noise ratio used here is a narrowband ratio of two Fourier amplitudes, rather than the wideband ratio of peak to root-mean-square amplitude used to measure gain. The narrowband ratio is strongly dependent on the distribution of signal and noise energy with frequency. The phase of the Love wave is arbitrary with respect to that of the vertical Rayleigh so the effective Love wave amplitude is smaller than that found from a spectrum.

We can get an idea of the best weighting function by calculating the distribution function of β for a few values of the signal-to-noise ratio in the range of interest. Such functions are shown in Figure IV-2 for narrowband signal-to-noise ratios of 4, 2, 1, 0.5, and 0.25, corresponding to wideband signal-to-noise ratios from about 20 to -4 dB for a typical test event and noise sample used here.

The weighting function was chosen to be the one shown in Figure IV-3 with center point $\theta = 0.0^\circ$ for frequencies between 0.024 Hz and 0.059 Hz and zero outside that passband. The probability of getting any useful information at frequencies where the signal-to-noise ratio is less than about one can be seen to be very small from Figure IV-2 so these frequencies outside the signal band are ignored.

The Rayleigh wave filter was designed in much the same way. Figure IV-4 shows the relevant angles, which are now in phase space rather than coordinate space as for the Love wave filter. The equation for the angle ψ , which is just 90 degrees for pure Rayleigh waves, is

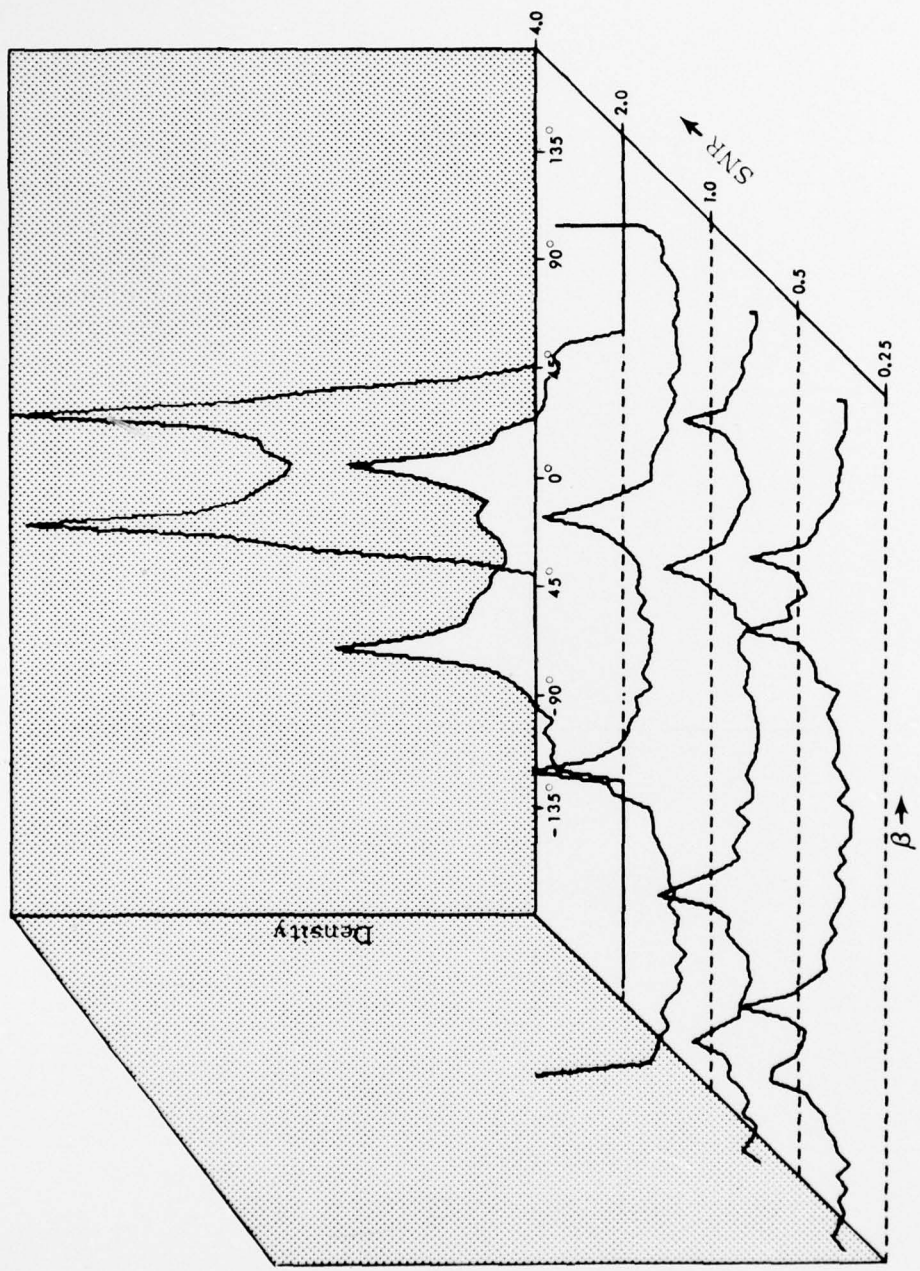


FIGURE IV-2
PROBABILITY DISTRIBUTION FUNCTIONS FOR β

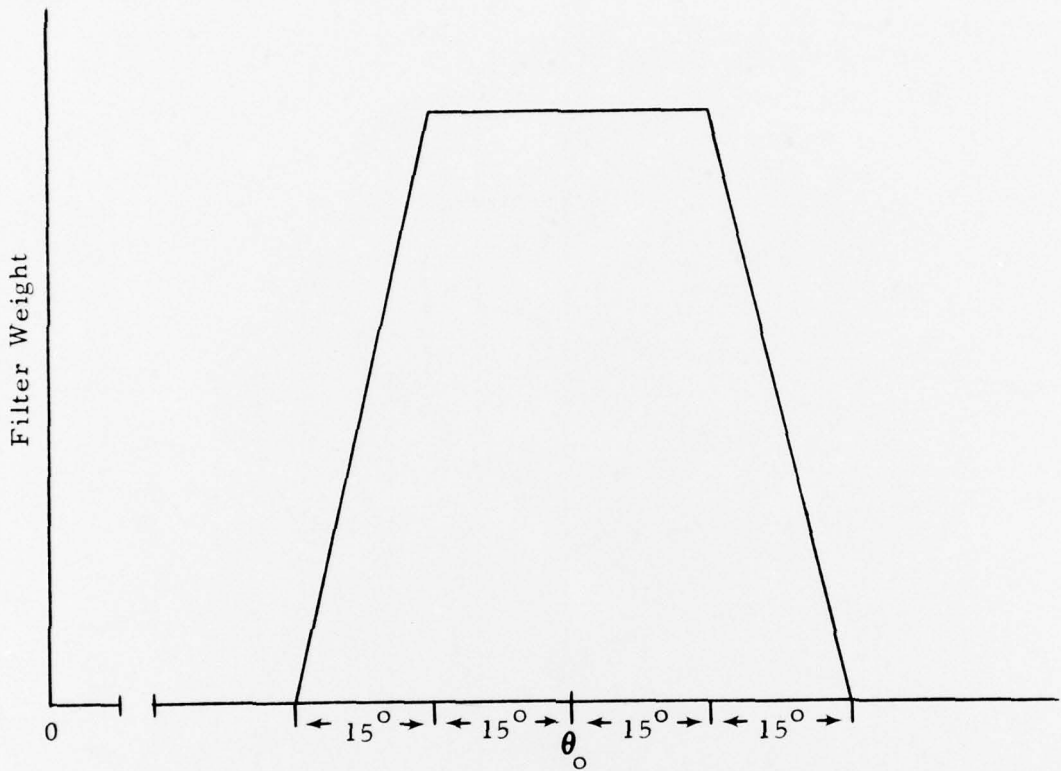


FIGURE IV-3
TCA WEIGHTING FUNCTION

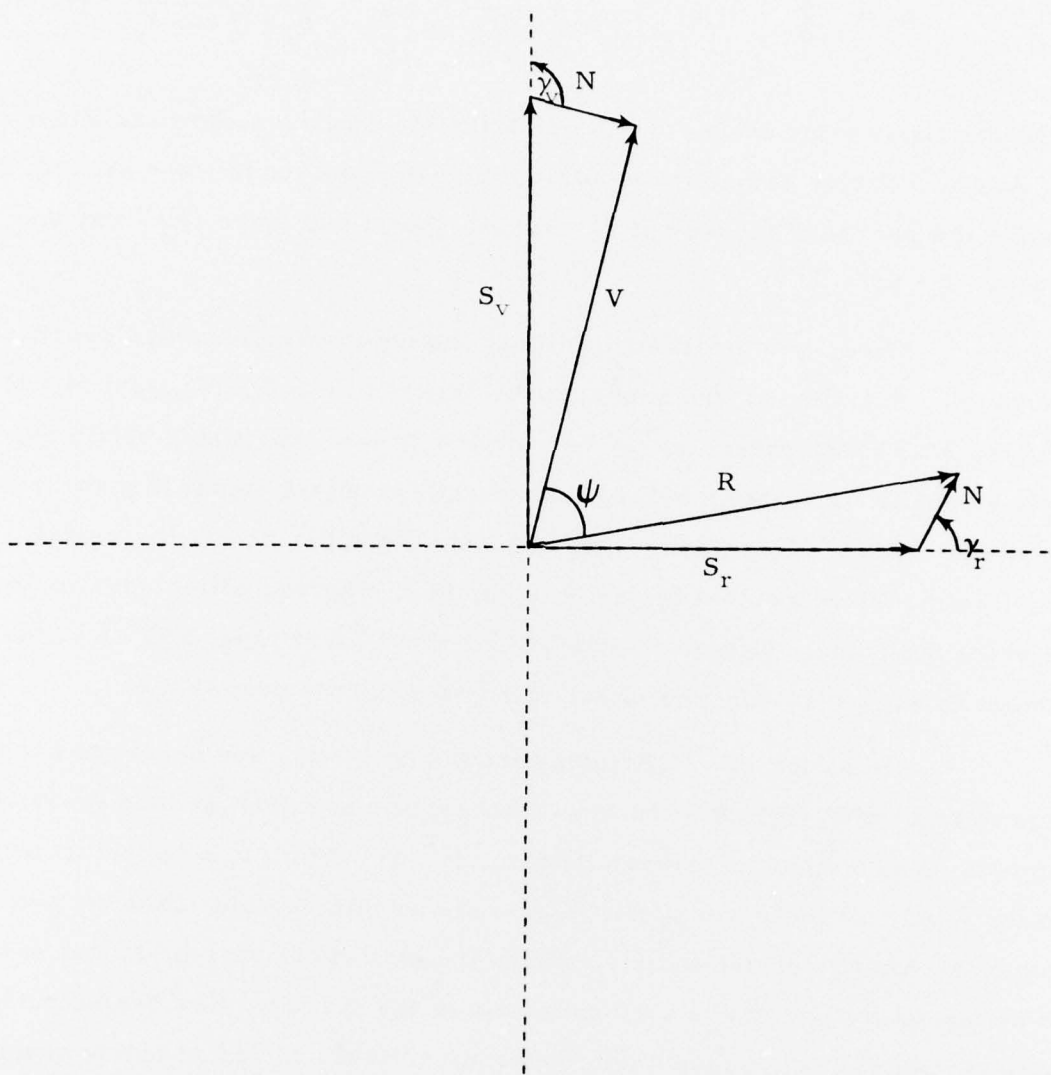


FIGURE IV-4
RAYLEIGH WAVE FILTER DESIGN

$$\psi = \frac{\pi}{2} - \tan^{-1} \frac{N \cos \gamma_v}{S_v + N \cos \gamma_v} - \tan^{-1} \frac{N \cos \gamma_r}{S_r + N \cos \gamma_r} \quad (\text{IV-2})$$

and a Monte Carlo simulation gave the distribution functions shown in Figure IV-5. Again, Fourier components outside the usual passband were zeroed, and inside the passband the weighting function shown in Figure IV-3 was applied with $\theta_0 = 90^\circ$.

Three combinations of signal and noise samples were processed, as usual. The results are presented in Figures IV-6 for constant signal and Figure IV-7 for constant noise. As for the Wiener and matched filters, there is stronger correlation between curves for constant signal than for ones with constant noise. Presumably this is because one signal fits the model used to find the filter weights better than another, whereas all noise samples agree about the same. Output waveforms for the TCA at input SNR of 10 dB are shown in Figure IV-8. The effect of segmenting the data is clear.

Gains for the TCA varied from 9 to 17 dB, and occurred over a range of input SNR from 8 to 16 dB. These gains are greater than those obtained from the matched or Wiener filters. It may be that this superior performance is due to the fact that the TCA needs no information about the phase or amplitude spectra of the signals, which are statistical variables, but depends on quantities which are true constants of the motion. For example, it is more certain that the phase angle between vertical and radial components is 90 degrees for Rayleigh waves than that the power spectrum takes on a given value at 20-second period for events from Kamchatka.

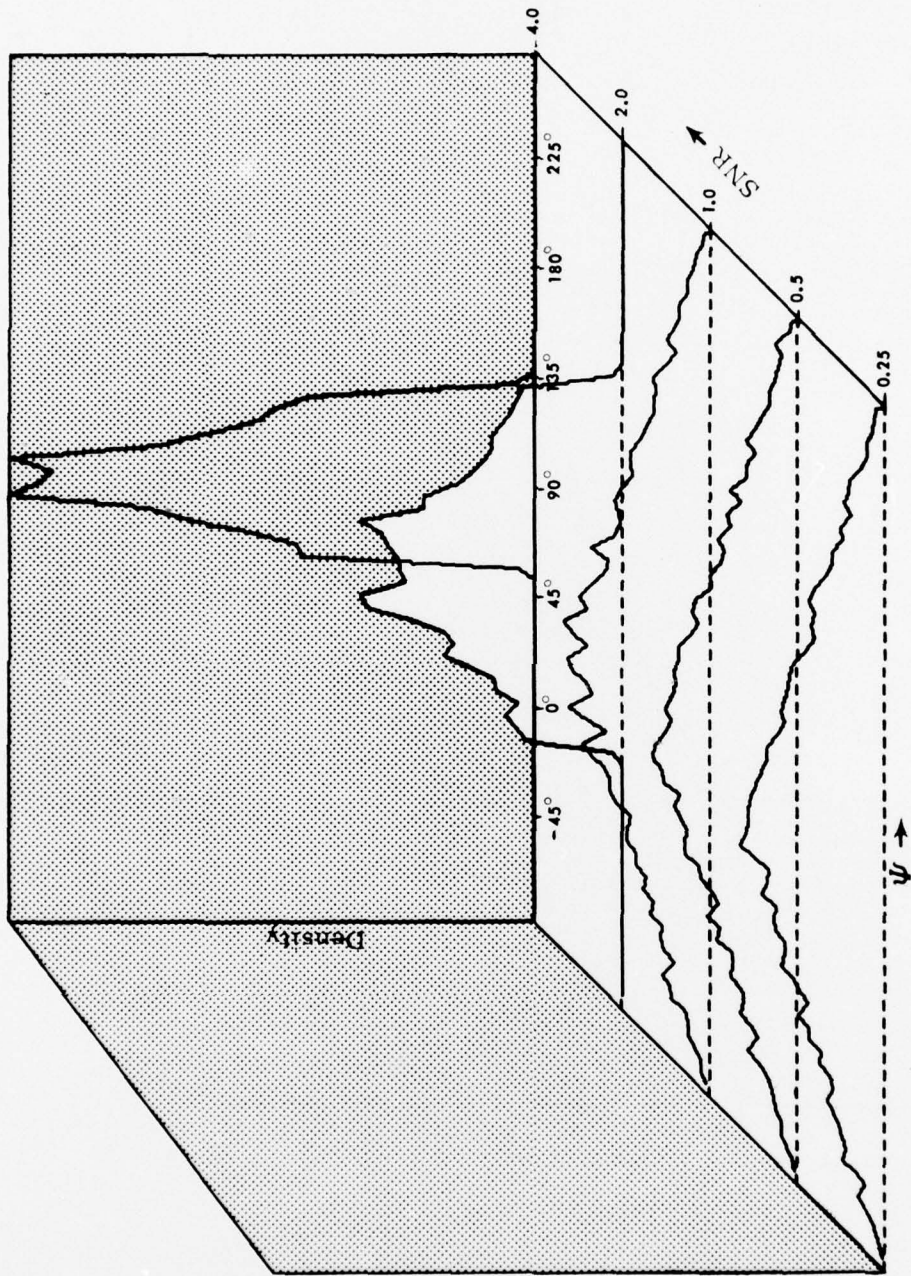


FIGURE IV-5
PROBABILITY DISTRIBUTION FUNCTIONS FOR ψ

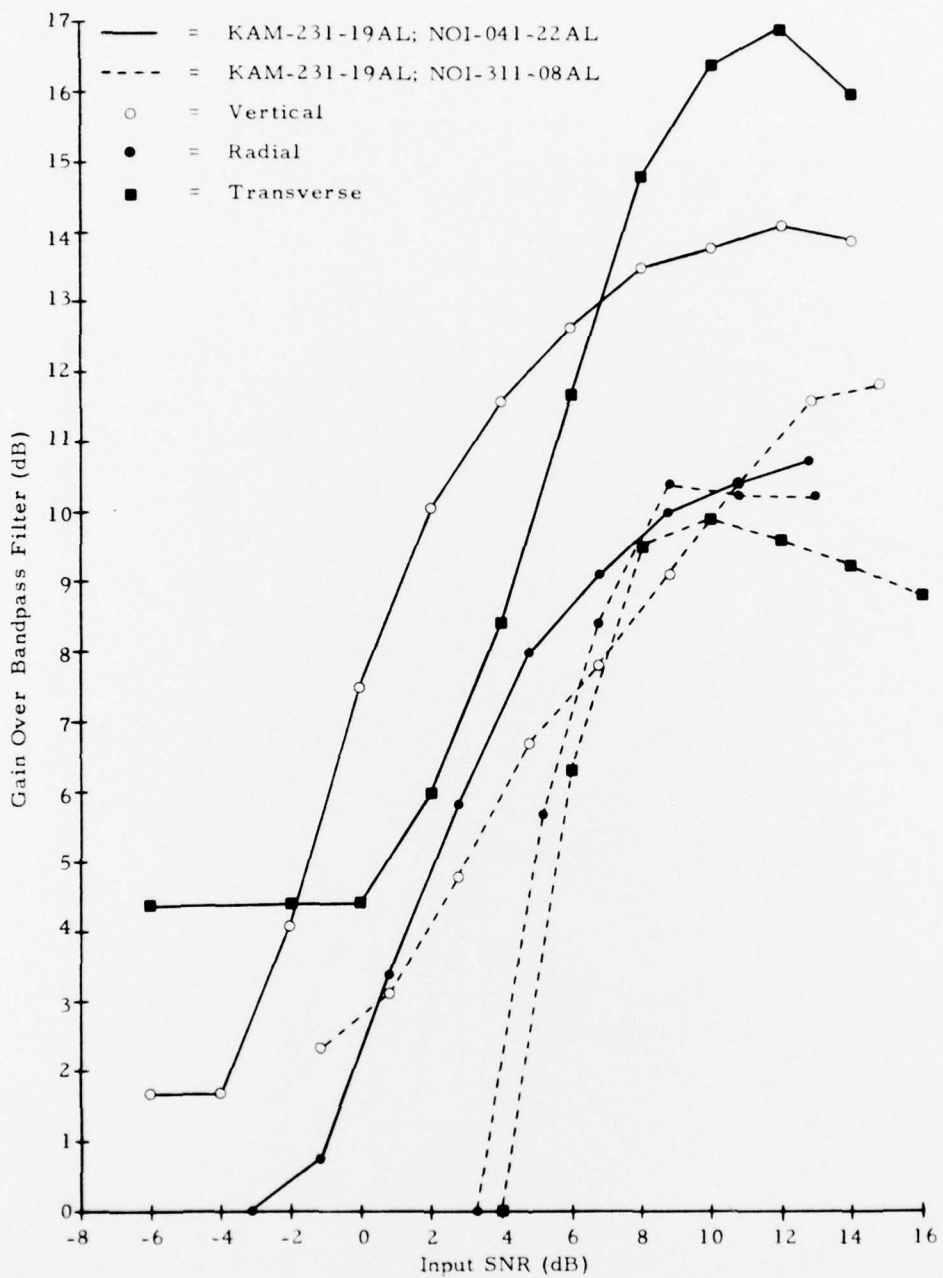


FIGURE IV-6
GAIN VERSUS INPUT SNR FOR TCA
WITH CONSTANT SIGNAL

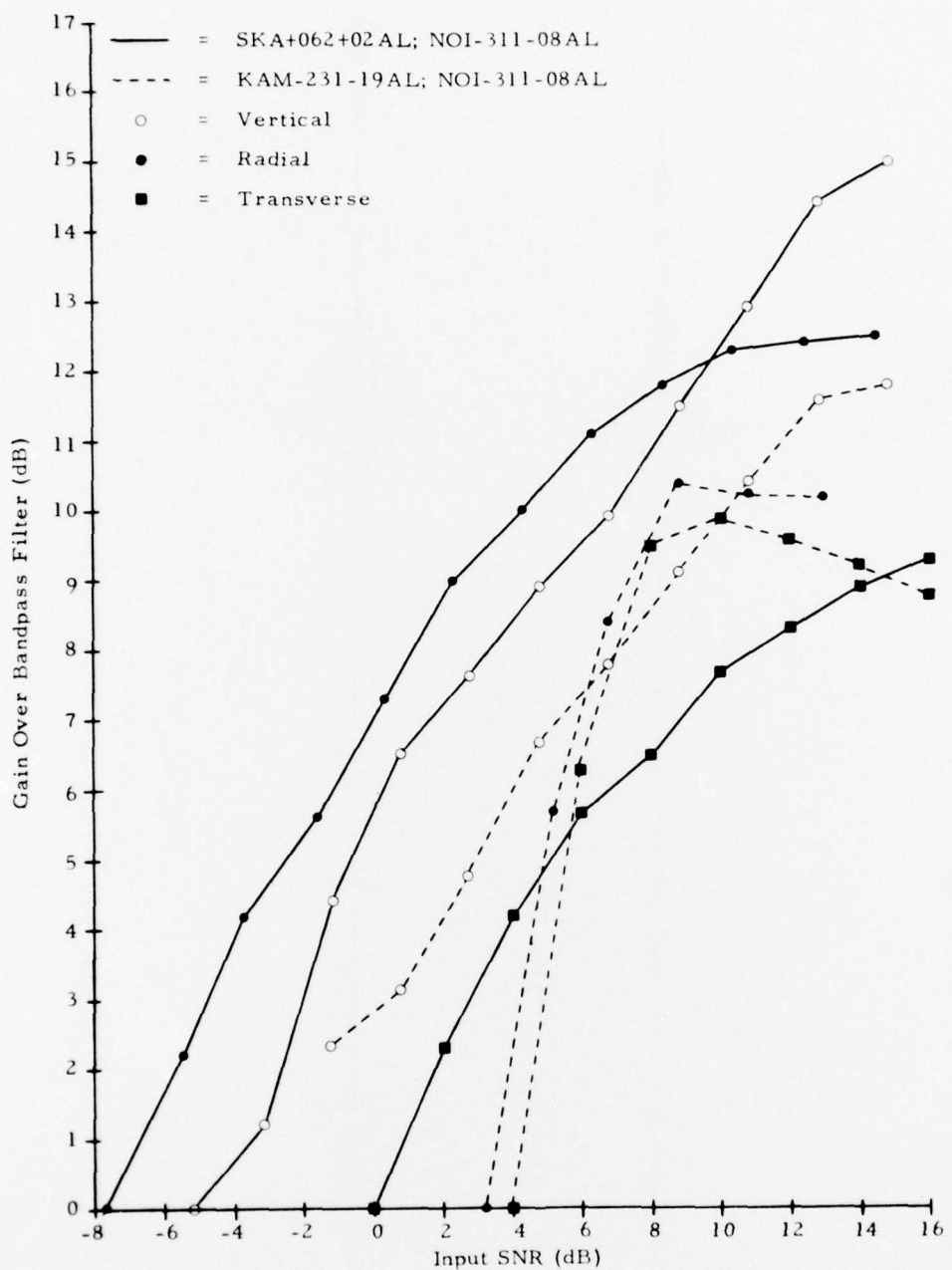


FIGURE IV-7
GAIN VERSUS INPUT SNR FOR TCA
WITH CONSTANT NOISE

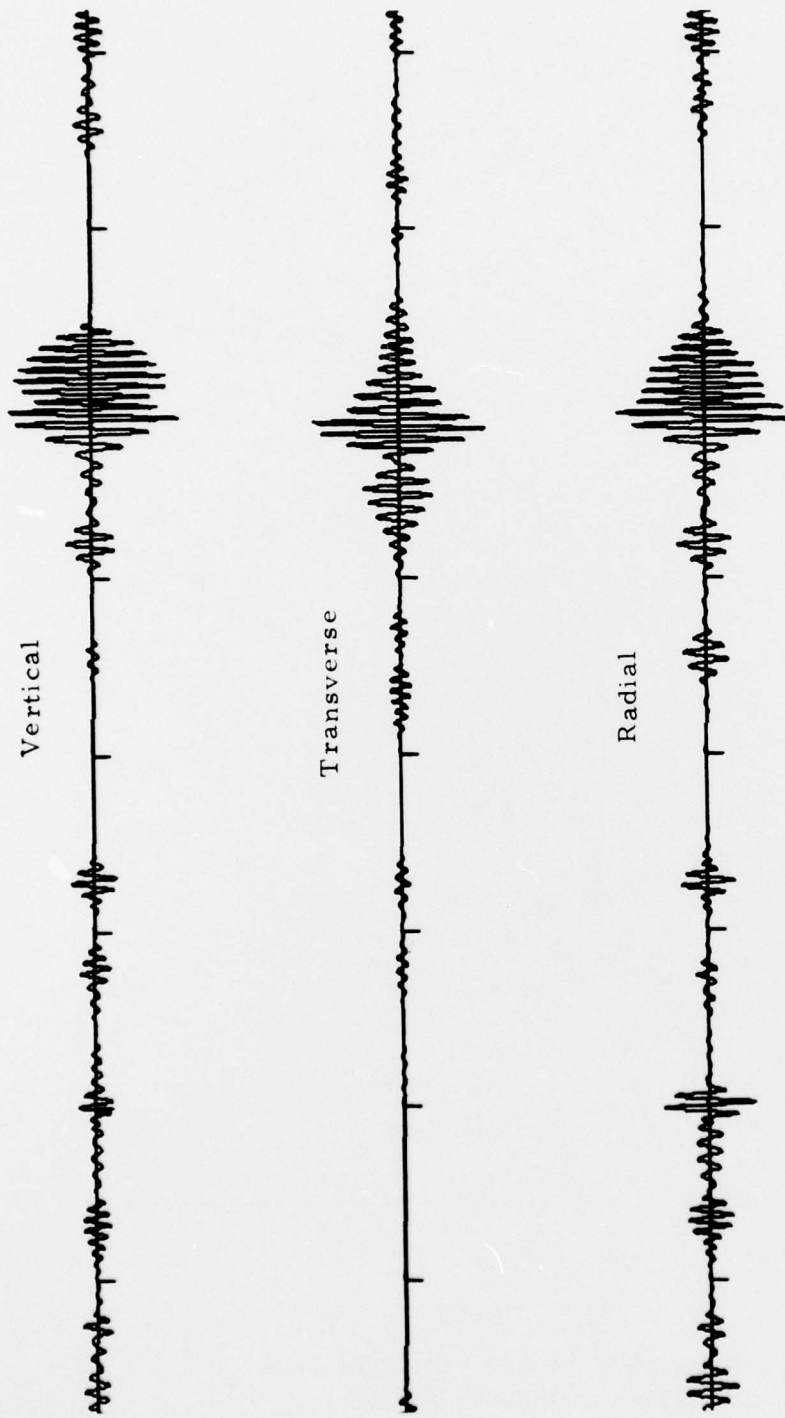


FIGURE IV-8

TCA OUTPUTS
(KAM-231-19AL IN NOI-311-08 AL)

SECTION V CONCLUSIONS

In this report the performance of three processors for single-site seismic data is presented. The processors are the Wiener filter, the matched filter, and the three component adaptive filter. Signals were buried in noise at known signal-to-noise ratios, and the outputs of the processors were compared to that of a bandpass filter.

The Wiener filter used a synthetic reference power spectrum and had its greatest improvement in signal-to-noise ratio when correlation terms between the signal and noise were ignored. The gain of this filter over the bandpass filter ranged from 2 to 6 dB, depending on the noise and signal samples examined.

A prewhitened matched filter using the same reference event (as the Wiener filter) displayed from 6 to 10 dB improvement over the bandpass filter. By the nature of the matched and Wiener filters, the matched filter is expected to have better gain.

The three component adaptive filter yielded from 10 to 17 dB improvement over the bandpass filter when a weighting function based on the probability distribution function of the variables of the surface wave particle motion was employed.

For all processors the gains found when signals were held constant were more consistent than when noise samples were held constant. This is presumably because details of the noise are less important in determining gain than are details of the signal being sought.

SECTION VI
REFERENCES

- Capon, J., R. J. Greenfield, and R. T. Lacoss, 1969, Long-Period Signal Processing Results for the Large Aperture Seismic Array, *Geophysics*, 34, 305-329.
- Strauss, A. C., 1976, Evaluation of the Improved Three Component Adaptive Processor, Technical Report No. 7, Texas Instruments Report No. ALEX(01)-TR-76-07, AFTAC Contract Number F08606-76-C-0011, Texas Instruments Incorporated, Dallas, Texas.